Effect of slip distribution on nearfield tsunami amplitudes; the 1952 Kamchatka earthquake

Breanyn MacInnes
June, 2007
Non-thesis Master's project

Abstract

We use the 1952 Kamchatka earthquake (M_w 8.8-9.0) and tsunami to explore the effect that internal slip distribution within a rupture has on tsunami amplitude in the nearfield. Our approach is to compare simulated tsunamis from 1952 Kamchatka with deposits in order to identify areas of high slip. Spatial variations in slip during tsunamigenic earthquakes result in variation in tsunami amplitude in the nearfield. Tsunami deposits from the 1952 Kamchatka earthquake and tsunami indicate that the tsunami was a minimum of ~ 20 m in southern Kamchatka and the northern Kuril Islands, as opposed to ~5-10 m in other nearfield coastal areas. Modeling of tsunami propagation from potential slip distributions show that in order to create the tsunami deposits and reported tsunami observations, the 1952 earthquake had regions of high slip off the coast of southern Kamchatka. Modeling further indicates that peaks in nearfield tsunami amplitudes generally occur adjacent to regions of high slip on the subduction zone. Changes by at least a factor of two in the amount or location of slip has noticeable effects on the coastal runup of simulated tsunamis, while smaller scale changes do not significantly alter the variation in nearfield tsunami amplitude.

1 Introduction and background

As demonstrated in 2004, tsunamis that accompany great subduction-zone earthquakes are a highly destructive natural force which can cause large numbers of casualties in coastal communities. Education and awareness combined with mitigation efforts are recognized ways to reduce a population's vulnerability to tsunami disasters (Bernard et al., 2006). Since the 2004 Indian Ocean tsunami, communities around the world have been working toward the goal of tsunami preparedness. At the heart of these efforts are the questions *how often* will a tsunami occur and *how big* will it be. Answering the question of *how often* requires the study of the past. For many parts of the world, paleotsunami deposits provide the most reliable archive of recurrence intervals because historical records are often short (e.g. Pinegina and Bourgeois, 2001; Kelsey et

al., 2002; Cisternes et al., 2005; Nanayama et al., 2007). Tsunami size, or *how big*, also can be determined with tsunami deposits (e.g. Nanayama et al., 2003, 2007; Satake et al., 2005) and historical tsunami surveys (c.f. Bourgeois, *in press*). However, as these studies are of the past, by themselves, they make few claims on predicting tsunami size for future events.

Tsunami amplitudes of future events are commonly predicted by forward modeling using numerical tsunami modeling (Titov et al, 2005). Tsunami models can routinely and reliably predict amplitudes of tsunamis in the farfield using location and seismic moment of an earthquake because with increasing distance from the source, perturbations in the waveform caused by the rupture are erased by bathymetry (Weiss, *in press*). Because initial perturbations are erased with distance, many forward models use generic uniform ruptures to determine potential tsunami amplitudes (e.g. Titov and Gonzales, 1997; Titov et al., 2001; Titov et al., 2005). However, nearfield tsunami amplitudes are strongly affected by earthquake characteristics such as the slip distribution along the rupture length (e.g. Geist and Dmowska, 1999; Geist, 2002); as every earthquake is different, so also will every tsunami be different. Without first determining and including earthquake characteristics important in altering tsunami amplitudes for a region, using forward tsunami models to predict the size of the tsunami in the nearfield can be misleading.

For past events, tsunami deposits are an potential resource for determining rupture characteristics that were important in past events. The most basic information derived from a tsunami deposit is 1) a tsunami must have reached the location of the deposit, and 2) the deposit's elevation is a minimum estimate of the peak tsunami amplitude at that

specific location. These basic interpretations require nothing beyond tsunami deposit identification and can be used to determine regional variations in the magnitude of a tsunami. The size of the tsunami can then be inverted to the initial sea floor disturbance and rupture characteristics of the earthquake.

1.1 Factors in local tsunami amplitude variations

For any given seismic moment, nearfield tsunamis can be significantly influenced by depth of rupture and amount and distribution of slip (Geist and Dmowska, 1999; Geist, 2002). Heterogeneous rupture patterns are expected for all earthquakes, but are more noticeable in large events (c.f. Johnson et al., 1996; Ishii et al., 2005). Geist (2002) ascribes a factor-of-three variation in peak tsunami wave heights in the nearfield to differences in earthquake slip distributions for a M_w 8.1 earthquake. Besides seismic moment, the most important means by which different earthquakes produce different tsunamis are 1) high slip and low shear modulus along the shallowest sections of the subduction zone, 2) variations in water depth in the rupture area, and 3) a heterogeneous slip distribution reflecting both depth and along-strike variations of the rupture (Geist, 2002). The first parameter set is responsible for a *tsunami earthquake* (Kanamori, 1972; Geist and Dmowska, 1999). The second parameter, local bathymetry, causes variations or perturbations in the initial waveform and propagation of the tsunami wave. Depth heterogeneities affect the vertical displacement field and generates different initial wave profile than homogeneous ruptures. Variations in slip along-strike result in spatial amplitude changes along the wavefront (Geist and Dmowska, 1999).

1.2 1952 Kamchatka background

We use the 1952 Kamchatka earthquake (M_w 8.8-9.0) (Fig. 1) and tsunami to explore the effect that internal slip distribution within a rupture has on tsunami amplitude in the nearfield. The 1952 Kamchatka earthquake began at 16:58:22 GMT on November 4th. The following tsunami had measurable runup around the world and was particularly destructive in the nearfield, destroying many of the villages and towns along the Pacific coastlines of southern Kamchatka and the northern Kuril Islands (Zayakin and Luchinina, 1987). Reported or accessible local observations are limited by a dispersed and military population. The earthquake and tsunami occurred at the height of the Cold War; direct observations and human experiences from Kamchatka and the Kurils of the earthquake and tsunami only recently are becoming available to the rest of the world (c.f. Zayakin and Luchinina, 1987; Nikonov, 2006).

The November 1952 Kamchatka earthquake (Fig. 1) is considered the fourth-largest historical event, including 2004 Indian Ocean (Brune and Engen, 1969; Kanamori, 1976; Okal, 1992; Lay et. al., 2005) and it has been relatively well-studied seismologically (c.f. Hutchinson, 1954; Hodgson, 1956; Brune and Engen, 1969, Kelleher and Savino, 1975; Kanamori, 1976; Johnson and Satake, 1999, Bürgmann et al., 2005). These studies constrain the earthquake's location and magnitude, but because of data and technology limits in 1952, the error range is large by today's standards.

For the 1952 earthquake, the generally accepted rupture area (Fig. 1) is approximately 700 km long, from northern Onekotan Island (49°N) to Shipunskii Cape (52.5°N), and 150-200 km wide. A cluster of foreshocks occurred near both the epicenter and the southern end of the rupture zone (Kelleher and Savino, 1975; Balakina, 1993).

Aftershocks within one month of the earthquake (Fig. 2) have been used to define the northern limit of the rupture (Ben-Menahem and Toksöv, 1963; Kelleher and Savino, 1975; Fedotov, 1982). Early studies proposed a rupture area 1000 km by 250 km (Bath and Benioff, 1957) but the larger area is considered to include earthquakes that are not aftershocks (Ben-Menahem and Toksöv, 1963). Slip direction appears to be perpendicular to the subduction zone (Kanamori, 1976).

The amount and distribution of slip are less certain than the location. There are relatively few records of the earthquake, some of questionable quality (Kanamori, 1976). Different analyses of even the same records (e.g. Kanamori, 1976; Okal, 1992) yielded different earthquake magnitudes. Estimates of seismic moment range from 180 to 350 x 10^{20} Nm, corresponding to a moment magnitude between M_w 8.84 and M_w 9.03 (Johnson and Satake, 1999). Original studies considered the earthquake to have ~5 m of homogeneous slip over the entire area (e.g. Kanamori, 1976). In contrast to this early work, Johnson and Satake (1999) calculated heterogeneous slip on possible 100 x 100 km segments by inverting tide gauge records of the tsunami waves from the farfield. They proposed a varying slip of up to 11.4 m, with large error ranges; high coseismic slip was predicted to have occurred only in sections of the subduction zone deeper than ~20 km (Fig 2). This depth of high slip, as analyzed by Johnson and Satake, makes the 1952 earthquake anomalous for tsunamigenic subduction-zone earthquakes in that the largest amount of slip ($\geq$ 5 m) does not occur near the trench (Bürgmann et al., 2005). Earlier studies of 1952 seismic records similarly suggest a deeper-than-average subduction-zone event— up to 40 km (Hutchinson, 1956) or 60-80 km (Ben-Menahem and Toksöv, 1963).

Heterogeneous patterns of slip distribution are thought to be largely controlled by the distribution of locked regions within the subduction zone. Using GPS measurements and the analyses of Johnson and Satake (1999), Bürgmann et al. (2005) identified 2-3 potentially persistent locked regions in the Kuril-Kamchatka subduction zone. Regions calculated by Johnson and Satake (1999) to have slip $\geq$ 5 m and determined by Bürgmann et al. (2005) to be currently locked zones correspond to the locations of large ($M_w \geq 7.0$) historical earthquakes. An area with ~10-12 m of slip corresponds to three 1904 and two 1993 earthquakes, another area with ~10-12 m slip corresponds to the 1973 earthquake, and the ~6-8 m slip area corresponds to the 1959 earthquake. Also, Johnson and Satake's areas with the highest proposed slip ($\geq$ 10 m) have a notably low count of aftershocks from 1952 (Fig. 2), supporting the idea that these regions re-locked immediately after rupture.

The 1952 Kamchatka earthquake produced a large tsunami which left deposits all along the Pacific coasts of central and southern Kamchatka and the northern Kuril Islands. These deposits are extensive, sometimes reaching kilometers inland and are old enough to be buried and preserved in stratigraphy. Moreover, the event is recent enough to make identification of deposits as from 1952 relatively straight forward.

2 Tsunami deposits as observations of the tsunami

2.1 Tsunamis create sedimentary deposits

The most fundamental information derived from a tsunami deposit is that a mapped deposit is less than or equal to tsunami inundation. Tsunamis create sedimentary

deposits as they flood the coast with high-velocity, turbulent, and sediment-rich water. Large tsunamis have the capacity to transport sediment kilometers inland over low gradients of topography (c.f. Dawson et al., 1988; Nanayama et al., 2003, 2007). Early studies of coastal paleo-tsunami deposits illustrated a link between coastal sand sheets and impulse-generating events such as earthquakes and landslides (Atwater, 1987; Dawson et al., 1988). Many post-tsunami surveys of modern tsunami deposits have been conducted, (Bourgeois, *in press*) showing that tsunamis can create a variety of sedimentary deposits. However, the general characterization of a tsunami deposit is a sand sheet that thins and sometimes fines landward, and that rises in elevation with topography away from the coast (Dawson and Shi, 2000). The general characterization holds true for modern tsunami deposits and buried, preserved paleotsunami deposits.

Modern and paleo-deposit surveys suggest that the form and lateral extent of a tsunami deposit is the result of a variety of factors. Many characteristics, from sediment availability to coastal topography to the velocity profile of the incoming and outgoing waves, play a role in sedimentation. In comparing specific locations, more extensive deposits are found where tsunamis overtop erodible beach ridges and coastal dunes (Bourgeois et al., 1999; Chadha et al. 2005); along rocky coasts, a tsunami of equal magnitude may leave no distinguishable deposit (Dawson and Shi, 2000).

2.2 Identification of deposits

There are a variety of characteristics helpful in distinguishing a tsunami deposit from other stratigraphic units in a coastal soil profile. In coastal plains, deposits generally are composed of sand, as the source of the sediment entrained in the tsunami is

primarily the sandy shoreface and nearshore. The type-case tsunami deposit is a clean (lacking in soil development) sand layer in otherwise non-sandy and/or soily stratigraphy (Clague et al., 1994; Minoura et al., 1996; Bourgeois et al., 1999; Dawson and Shi, 2000; Nanayama et al., 2003; Pinegina et al., 2003). Limited soil development within the layer is due to rapid accumulation of the deposit. Besides being clean and sandy, tsunami deposits may have an erosive base and exhibit normal, or sometimes inverse, grading (Bourgeois et al., 1999; Hindson and Andrade, 1999; Dawson and Shi, 2000; Bondevik et al., 2005). A tsunami deposit can also contain rip-up clasts of peat, turf, or soil, as well as sediment coarser than sand, depending on the grain-size distribution of the sediment source (Dawson and Shi, 2000; Nanayama et al., 2003; Bondevik et al., 2005). For example, in the volcanically active Kamchatka and Kuril Islands, large clasts of rounded pumice are common in tsunami deposits.

Many of the above characteristics are not limited to tsunami deposits. Other mechanisms such as storms, floods, eolian processes and volcanic processes are capable of producing sand sheets in coastal-plain stratigraphy, thus requiring the application of additional criteria for defining a tsunami deposit. Therefore, we avoided locations where storms or floods could deposit sand layers such as near levee braches or low areas near the shore. Similarly, eolian activity may produce clean sand layers locally resembling tsunami deposits. However, eolian deposits are generally better sorted and less sheet-like than tsunami deposits. Volcanic processes can also generate sandy tephras, but these sand sheets exhibit more uniform mineralogy and grain size, whereas sediment of a tsunami deposit reflects the mineralogy of whatever the tsunami traveled over, such as a bay, beach, or river channel.

2.3 Identification of deposits as from 1952

Dating a deposit as from the 1952 Kamchatka tsunami in our study relies on relative dating techniques. The most accurate technique we use is the stratigraphic relationship of the deposits to historical volcanic tephra or to other historical material. Recent tephra within the field areas are 1981 Alaid and 1986 Chikurachki tephras on Paramushir and Shumshu islands (Fedotov et. al, 1981; Ovsyannikov and Muraviev, 1992), and 1907 Ksudach tephra and 1945 Avachinski tephra in northern field locations (Braitseva et. al, 1997; Melekesev et al, 1994). Also, materials found in deposits or adjacent stratigraphy, such as boat debris, metal, cut logs, glass, plastic, etc. (c.f. Nanayama et al., 2000) can help provide a datum.

In lieu of datable components in the stratigraphy, sand sheets were identified as 1952 by reference to their stratigraphic position relative to the modern surface, by the amount of overlying accumulation and soil development, by their thickness relative to other deposits, and by their continuity. The 1952 tsunami is the most recent event within the field area that was capable of inundating far beyond the supratidal zone (Table 1). It is the most recent tsunami to have recorded heights >5 m in this region (the 1960 Chile tsunami is only reported >5 m in one location in the field area (Zayakin and Luchinina, 1987)). The next older tsunami of potentially comparable size is the 1841 or the reported 1737 events (Zayakin, and Luchinina, 1987). Therefore, if present, the 1952 deposit will be the tsunami deposit closest to the surface at elevations >5 m. At elevations <5 m, there can be many sand layers near the surface because of storms and other tsunamis. In

these instances, the 1952 deposit can be correlated between excavations using stratigraphic position, thickness, grain size and mineralogy.

Unsurprisingly, some excavations yield inconclusive results. For example, an excavation may contain a large amount of sand, making the identification of tsunami deposits as distinctive units difficult. Also, the original sand sheet may have been deposited as a very thin layer in some areas, which, through time and bioturbation, may not remain as a coherent, clean sand layer. Due to these and other stratigraphic uncertainties, excavations with ambiguous descriptions were counted as not containing the 1952 deposit for the purpose of this study.

2.4 Tsunami deposits define a minimum wave height

Tsunami deposits can estimate the minimum distance and elevation a tsunami traveled because sediment generally cannot be carried and deposited at the farthest extent of the tsunami. A tsunami will lose its capacity to maintain sand-sized particles in suspension or to carry sand as bedload some fraction of time before it ceases to travel inland. The *tsunami deposit estimate* (TDE) we use in this paper is the elevation of the highest tsunami deposit (Fig. 3). As such, it is the largest approximation for the more commonly used *runup* of the tsunami that can be estimated with sediment. The presence or absence of sediment provides evidence of a location being underwater. Any interpretation beyond that requires many assumptions. The TDE is equally a function of the size of a tsunami as *runup*.

Through identification and mapping of 1952 deposits over seven summers of working in Kamchatka and the Kuril Islands, we calculated the TDE for 34 locations.

We identified these deposits in excavations dug along topographic profiles measured perpendicular to the shoreline using hand levels and/or transit levels (Fig. 3a). Elevation and distance inland of deposits were calculated from high-high tide, being the position common to all profiles. Field sites were primarily sandy coastal plains, such as beach-ridge sequences, where the availability of sand maximized the likelihood of generating and preserving tsunami deposits.

We determined the TDE for 1952 Kamchatka by placing the presence or absence of distinct 1952 deposits in the context of the topographic profiles (Fig. 3). The tsunami flooded to at least the highest excavation with a 1952 deposit, making the elevation of that excavation the TDE for a specific profile. Higher topography in a profile without excavations were not accounted for in the TDE because the tsunami did not necessarily traverse a direct path. We made a distinction between profiles where the farthest landward excavation still contained the 1952 deposit and ones that did not (Fig. 3). If there was no deposit in the last excavation, then the limit of sediment inundation likely occurred within the measured profile and the TDE is likely close to the actual tsunami runup, especially in relatively flat coastal plains. For profiles where 1952 extends beyond all excavations, the actual size of the tsunami could be much greater than the TDE, as topography landward of the profile is unknown.

2.5 Results of tsunami deposit and reported observation elevations (TDE)

Field observations of 1952 tsunami deposit elevations and locations define the trend of tsunami amplitudes from Kamchatka and Kuril coastal lowlands (Fig. 3b). Higher deposits were observed adjacent to the southern half of the rupture area. In the

north, around Khalaktirka, the TDE is 3-6 m above high-high tide. Between Avacha Bay and Vestnik Bay, the TDE is at least 5-8 m, with a maximum at Mutnaya Bay of 11 m. Data are sparse north and south of Khodutka because of limited coastal lowlands. From Vestnik Bay to northern Paramushir, TDE observations vary widely between 2 and 19 m, although more than half the locations have values >10 m. The very southern end of the rupture zone indicates TDE values of a minimum of 7-8 m.

Individual TDE values in Figure 3b vary in elevation over short distances because each estimate is strongly influenced by topography. A profile only has the potential to preserve a deposit up to its highest elevation. The same tsunami can produce highly variable TDE estimates if topography is equally as variable. Profiles from the same locality with higher estimates are likely more reliable representations of tsunami amplitude.

We used the highest TDE from each embayment or general area to define the trend of estimated tsunami wave heights along the coast of Kamchatka and the Kurils. The resulting pattern (Fig. 3b) indicates that the amplitude of the 1952 tsunami was two or three times greater in southern Kamchatka and the Kuril Islands than in the northern end of the rupture zone. This disparity is reinforced by the observation that the limits of sediment inundation were observed in most northern profiles but were not reached in the south (Fig 3b). Thus, TDE values from the south are more likely to underestimate tsunami runup; if the southern profiles extended farther landward to the sediment inundation limit, the maximum deposit elevation could only be higher. Reported observations from 1952 (Zayakin, and Luchinina, 1987) are included in creating the general trend of estimated tsunami wave heights and show a similar trend as the deposits

(Fig. 3b), with the highest wave arriving in the vicinity of northern Paramushir and Shumshu.

3 Modeling the tsunami and earthquake slip distribution

3.1 MOST tsunami propagation and runup model

In order to relate tsunami deposits to characteristics of the an earthquake, we must have a method of generating and propagating a tsunami from a seafloor displacement. NOAA's Method of Splitting Tsunami (MOST) model (Titov and Synolakis, 1995, 1998; Titov and Gonzales, 1997) is a standard forecasting model which can perform those functions for a theoretical earthquake. The MOST model uses non-linear shallow-water wave equations to propagate an impulse-generated wave across a set bathymetry (Titov and Synolakis, 1998). The shallow-water wave equations are in the form:

$$h_t + (uh)_x + (vh)_y = 0 \quad (1a)$$

$$u_t = uu_x + vu_y + gh_x = gd_x \quad (1b)$$

$$v_t + uv_x + vv_y + gh_y = gd_y \quad (1c)$$

Where:

$h = \eta(x,y,t) + d(x,y,t)$

$\eta(x,y,t)$ = amplitude

$d(x,y,t)$ = undisturbed water depth

$u(x,y,t)$ and $v(x,y,t)$ = depth-averaged velocities

x = onshore

y = longshore

g = gravity

Runup is computed using the method described in Titov and Synolakis (1996). MOST has been successfully validated many times against laboratory experiments and field data (c.f. Titov and Synolakis, 1996, 1998; Bourgeois et al., 1999) and can reliably calculate runup (Titov and Synolakis, 1995). The equations have a moving boundary for inundation and have been shown to handle weakly breaking waves. Calculations of runup use moving boundary conditions and wave amplitude to convert "dry" points to "wet" points (Titov and Synolakis, 1998). However, during shoaling, wavelength shortens as water depth decreases and the equations loose accuracy and efficiency, depending on bathymetric and topographic grid resolution (Titov and Synolakis, 1995; Titov and Gonzales, 1997)

As such, high resolution bathymetry and topography is crucial for accurate runup modeling. We converted the bathymetry and topography data for the Kuril and Kamchatka area into a 120" (2.4-3.7 km) resolution grid covering the entire Kamchatka and Kuril study area, and within the larger grid, a series of 30" (0.6-0.9 km) resolution grids which overlap to cover the Pacific coastline (Fig. 4). Telescoping grids decrease run time and allow for computation in complicated areas (Titov and Synolakis, 1998).

There is a pronounced difference in bathymetric profiles off the Kamchatka and Kuril Island Pacific coasts between the northern and southern extent of the 1952 rupture zone. In general, the continental shelf off south Kamchatka and the northern Kurils is long and broad with a uniform and gentle slope. The continental shelf from approximately Mutnaya Bay to Avacha Bay is narrow; the continental slope is very steep and trends almost north-south. Bathymetry from the northern end of the rupture zone

generally mimics the coastline— Shipunskii Cape extends eastward as a bathymetrically high area and Avacha Bay exits into a submarine canyon. Otherwise, the continental shelf width and gradient is in between those of the south and central regions.

A tsunami waveform approaching the Kamchatka shoreline is affected dynamically by the bathymetry. During propagation, having a narrower shelf in the north enables the wave to maintain faster velocities for longer. A wave generated from slip covering the entire rupture area arrives at the coast first in the northern region and the arrival time propagates down the coast. Bathymetry also causes tsunami amplitude to increase more seaward of the coast in the south than the north.

3.2 Slip distribution modeling

MOST uses the standard approach for determining seafloor and water-surface deformation (Titov and Synolakis, 1998). We manipulated potential slip distributions for the 1952 event by altering the source model in MOST. The source model is composed of a series of 100 x 50 km rectangles, or unit sources, which represent the subduction zone, and on which the amount of slip can be defined (Fig. 4). Vertical displacements are derived from equations presented in Okada (1985). Okada translates slip on a planar fault of a unit rectangular area into x, y, and z displacement at the surface of a homogeneous half-space.

A number of different slip distributions were run (Figs. 5-8), including reconstructions of Johnson and Satake's (1999) slip distribution pattern of 1952 Kamchatka. Tested hypotheses for slip distributions during the 1952 earthquake included homogeneous and heterogeneous patterns. We applied homogeneous (equal) slip to basic

distribution patterns of 1) the entire rupture zone— a 700-by-200-km rectangle (Fig. 5a-b), 2) slip concentrated either in the shallow or deep section of the subduction zone— 700-by-100-km rectangles (Fig. 5c-d), or 3) slip concentrated in strike-parallel groupings— 300-by-200-km rectangles (Fig. 6). We required that any rearrangement of the slip in the unit sources maintained a total magnitude between M_w 8.8 and 9.0. Heterogeneous slip distributions, with each unit source having different values for slip, we tested were based initially on the work of Johnson and Satake (1999) (Fig. 2) and included their error range (Fig. 7). In search of more accurate slip distributions, we also made modifications to the Johnson and Satake (1999) and homogeneous distributions (Fig. 8). Compared to each other, these modifications varied in that southern slip regions were extended to shallower regions of the subduction zone and/or were connected, and northern slip regions changed depth.

We compared simulated tsunami runup with minimum estimates of wave heights from tsunami deposits in order to assess the likelihood of potential slip distributions. We analyzed the model results to determine the *tsunami maximum amplitude* (TMA) of the simulated tsunami waveform for grid points with elevations between -1 and +50 m. The minimum distance between modeled grid points and every profile locations or cataloged observations was calculated in order to make the most direct comparison between model and observation. In general, locations with TDE values were reasonably close to a model grid point. TMA values for model grid points that were equidistant to TDE locations were averaged so a one-to-one comparison between modeled tsunamis and tsunami deposits could be made.

Using the direct comparison between model results and tsunami deposits we analyzed the capability of each slip distribution to create a simulated tsunami in agreement with TDE observations. Most importantly, modeled tsunami need to match the overall pattern from figure 3 of tsunami amplitude along the entire coast, as predicted by the TDE observation. A model also should explain the most number of observations; the TMA values must be equal to or higher than the TDE values otherwise the deposit could not have been created. Another important metric is how much the simulated tsunami over-predicts the deposits. For example, tsunami amplitudes that consistently reach many meters higher in elevation than the deposits is a worse fit than one that extends only a few meters, especially for profiles where the limit of sediment inundation is observed. Finally, to quantify the poor matches, we calculated the average underestimation of the TDE observations by the simulated tsunami.

4 The effects of slip distribution

4.1 Bathymetry

The zero-th order hypothesis for explaining the pattern of deposit elevation is that it is caused solely by the effect of bathymetry on local tsunami amplitude and runup. This hypothesis implies that slip distribution has no effect on nearfield tsunami amplitudes and, for the case of the 1952 Kamchatka event, deposits are higher in the south because the wave was amplified by bathymetry. We would expect to see that simulated tsunamis should be amplified consistently from northern Paramushir to Vestnik

Bay. However, if anywhere, tsunamis were only focused around Vestnik Bay, Zhirovaya Bay, and the mouth of Avacha Bay.

In our modeling efforts, bathymetry had an additional effect. Regions of anomalously shallow bathymetry made it impossible to produce large TMA values for any modeled slip distribution along the coast from the tip of Kamchatka and south. Modeled tsunamis have very high amplitudes over these offshore shallow areas which allows energy to dissipate before the coastline. Maximum values for Paramushir and Shumshu occur 5-6 hours after the earthquake potentially due to this dissipation and later resonance. If we remove the coastal regions adjacent to the anomalous bathymetry from the analysis, we can generally add ~10% to the number of deposits a source model can explain, as reported in Fig. 5-8.

4.2 Homogeneous slip distributions

Homogeneous slip distributions explored the effects of depth and along-strike location of high slip. We tested two slip distributions where the entire rupture zone moved an equal amount. A tsunami from 5 m of uniform slip (a M_w 8.8) is only large enough to produce 10% of the deposits (Fig. 5a); the remaining 90% of observations were > 8 m higher than modeled tsunami amplitudes. Increasing the slip to 9 m (M_w 9.0) had the effect of increasing the TMA (Fig. 5b), although not by a constant factor because tsunami runup is a non-linear process. This type of slip distribution showed that tsunamis generated from equal displacement in the entire rupture zone are roughly equal in size for the entire nearfield area— not the observed trend.

Concentrating slip in either the shallow or deep sections of the subduction zone had the effect of increasing tsunami amplitude from the previous distributions (Fig. 5c-d vs. 5a-b). In general, this may be due to the fact that slip doubles to 18 m (for a M_w 9.0 earthquake) in order to maintain the same magnitude because area decreases by half. The shallow slip concentration produced a larger tsunami than the deep because shallower ruptures create larger tsunamis than equal-magnitude deeper earthquakes (Geist, 2002). In general, the homogeneous slip distributions with slip extending the length of the rupture zone produced generally consistent TMA values between the northern and southern regions and changing the amount of slip did not significantly alter that pattern. Of all slip distributions modeled, the shallow depth concentration (Fig. 5d) would be able to produce more of the deposits than any other (69%). However, the wave exceeded deposits by 6.5 m on average and by 10-15 m in the north. Such a disparity seems unrealistic, especially in areas where the limits of sediment inundation are present. Also, the northern region is the most populated area of the coast and there is no known record of the wave being more than 8 m high there (Zayakin, and Luchinina, 1987).

Concentrations of uniform slip north or south in the rupture area have the effect of generating locally increased tsunami amplitudes (Fig. 6). Peak heights of TMA values correlate with the slip concentration except for high slip in the south (Fig. 6a-b), although, as mentioned previously, low amplitudes in the south are likely due to the anomalously shallow bathymetry. The strike-parallel slip concentration with slip localized immediately off southern Kamchatka (Fig. 6c) is the best match with the deposit data. It explains 39% of deposits but only over-tops deposits by an average of 3.0 m. This slip distribution is similar to the largest slip concentration suggested by Johnson

and Satake (1999) and corresponds to southern locked regions reported by Bürgmann et al. (2005).

4.3 Heterogeneous slip distributions

The heterogeneous slip distributions are based on the distribution determined by Johnson and Satake (1999) (Fig. 2). These distribution patterns (Fig. 7) have three primary areas of high slip, of which the southern two overlap with the best strike-parallel concentration (Fig. 6c). The third area at the northern end of the rupture zone also corresponds with a locked region suggested by Bürgmann et al. (2005). Adding the northern region of high slip does not improve the agreement between the TMA and TDE values over the strike-parallel distributions. Of the Johnson and Satake (1999) slip distributions, the M_w 9.0 preferred model (Fig. 7d) can produce the largest percent of deposits (37%). However, the overall pattern of a larger tsunami in southern Kamchatka is not as apparent in the Johnson and Satake distribution model runs; amplitudes at the northern end become proportionally too high. Therefore, the deposits suggest that the northern slip concentration may not have ruptured to the extent determined by Johnson and Satake (1999).

We also made subtle modifications of the Johnson and Satake slip distribution (Fig. 8) in order to test the responsiveness of tsunami amplitude to small-scale variations in slip— variations that may be difficult to detect seismically. The resulting TMA values overestimate the deposits by a smaller amount than the best-fit Johnson and Satake model (Fig. 7d) (2.6-3.5 m vs. 6.5 m) because the slip was more distributed. All modifications of the Johnson and Satake slip distribution were all able to explain 31% of deposits,

roughly on par with the best strike-parallel model (Fig. 6c). The TMA values were essentially identical between the three slip distributions; amplitudes for any given location varied by only a meter or two between the three models in figure 8.

5 Conclusions

The standard practice of assuming uniform slip over an entire rupture zone for tsunami models is not an adequate method for determining nearfield tsunami amplitudes. The earthquake slip distributions we tested reinforce the idea that the depth of slip strongly affects tsunami amplitude, although slip depth does little to alter regional wave-height differences (Fig. 5). However, changing the slip distribution along-strike (Fig. 6) can concentrate tsunami heights locally and create a larger tsunami immediately adjacent to the highest slip area. Small scale variations (Fig. 8) in slip do not change the initial tsunami waveform enough to result in significant differences in tsunami amplitudes at the coast, at least for large earthquakes. It may be that a M_w 9.0 earthquake is so large that small variations in slip distributions are proportionally minute.

For the specific case of 1952 Kamchatka, the TDE values clearly show much greater wave heights in southern Kamchatka and the northern Kuril Islands (Fig. 3) than at the northern end of the rupture zone. The variation in tsunami amplitude cannot be produced by a rupture pattern of equal slip the length of the rupture (Fig. 5). The general picture of slip from the 1952 event is of high slip off southern Kamchatka; a concentration of slip at the very northern end of the rupture zone may exists but is not proportionally as large as reported in Johnson and Satake (1999).

A relatively consistent observation that emerged from all the model runs, but was especially apparent in the Johnson and Satake model runs (Fig. 7), is that an earthquake smaller than M_w 9.0 is less able to produce the observed deposits. This conclusion reinforces the concept that paleotsunami deposits can be useful tools for constraining minimum magnitudes of paleo-earthquakes. However, there may be some questions as to the robustness of this conclusion due to the coarse resolution of the bathymetry and a limited understanding of the processes that result in deposit sedimentation.

For coastal regions without historical tsunamis, paleotsunami deposits are a valuable but underexploited source-model validation tool. Deposits can inversely predict regions of large coseismic slip. Using tsunamis to determine slip distributions can help constrain reduction in stress at the subduction zone (e.g. Hirata et al, 2003) and make predictions about future events (e.g. Johnson and Satake, 1997). Because high-slip regions are associated with locked sections of subduction zones, these regions may persistent in time and be useful for studies of pre- or post-events (Johnson and Satake, 1999; Bürgmann et al., 2005). For the case of Kamchatka, a larger tsunami in southern Kamchatka is likely to reoccur during the next large Kamchatka earthquake and tsunami.

Acknowledgements

This work was funded by the National Science Foundation (grant # EAR-0125787). Fieldwork was conducted by a many people under supervision of Tatiana Pinegina and Joanne Bourgeois. The MOST model and the unit sources were provided by the modeling group of the NOAA Center for Tsunami Research (PMEL-NOAA, JISAO-University of Washington). MOST programming was provided by Edison Gica. General programming help and patient instruction came from Robert Weiss.

Bibliography:

Atwater, BF, 1987, Evidence for Great Holocene Earthquakes Along the Outer Coast of Washington-State: Science, v. 236, p. 942-944.

Cisternas M, Atwater BF, Torrejon F, Sawai Y, Machuca G, Lagos M, Eipert A, Youlton C, Salgado I, Kamataki T, Shishikura M, Rajendran CP, Malik JK, Rizal Y, and Husni M, 2005, Predecessors of the giant 1960 Chile earthquake: Nature, v. 437, no. 7057, p. 404-407.

Balakina, LM, 1993, Kamchatka earthquake of November 4, 1952, and its position in the seismic events of the Kurile-Kamchatka Zone, Izvestiya - Russian Academy of Sciences. Physics of the Solid Earth, v. 28, no. 6, p. 459-471.

Bath, M, and Benioff, H, 1957, Aftershock sequence of the Kamchatka earthquake of November 4, 1952, Geological Society of America Bulletin, v. 68, no. 12, Part 2, p. 1819.

Ben-Menahem, A, and Nafi Toksoez, M, 1963, Source mechanism from spectrums of long-period surface waves; 2, The Kamchatka earthquake of November 4, 1952, Journal of Geophysical Research, v. 68, no. 18, p. 5207-5222.

Bernard, EN, Mofjeld, HO, Titov, V, Synolakis, CD, and Gonzalez, FI, 2006, Tsunami: scientific frontiers, mitigation, forecasting and policy implications, Philosophical Transactions of the Royal Society A, 364, doi:10.1098/rsta.2006.1809.

Bondevik, S, Lovholt, F, Harbitz, C, Mangerud, J, Dawson, A, and Svendsen, JI, 2005, The Storegga Slide tsunami— comparing field observations with numerical simulations, Marine and Petroleum Geology, v. 22, p. 195-208.

Bourgeois J, Petroff C, Yeh H, Titov V, Synolakis CE, Benson B, Kuroiwa J, Lander J, Norabuena E, 1999, Geologic setting, field survey and modeling of the Chimbote, northern Peru, tsunami of 21 February 1996: Pure and Applied Geophysics, v. 154, no. 3-4, p. 513-540.

Bourgeois, J., *in press,* The geologic effects and records of tsunamis, in Bernard, EN, and Robinson, AR (eds), The Sea, Volume 15, Harvard University Press.

Braitseva, OA, Ponomareva, VV, Sulerzhitsky, LD, Melekestsev, IV, and Bailey, J, 1997, Holocene Key-Marker Tephra Layers in Kamchatka, Russia, Quaternary Research, 47, 125-139.

Brune, JN, and Engen, GR, 1969, Excitation of Mantel Love Waves and Defiition of Mantle Wave Magnitude: Bulletin of the Seismological Society of America, v. 59, p. 923-934.

Bürgmann R, Kogan MG, Steblov GM, Hilley G, Levin VE, and Apel E, 2005, Interseismic coupling and asperity distribution along the Kamchatka subduction zone: Journal of Geophysical Research-Solid Earth, v. 110, art. no. B07405.

Chadha RK, Latha G, Yeh H, Peterson C, and Katada T, 2005, The tsunami of the great Sumatra earthquake of M 9.0 on 26 December 2004 - Impact on the east coast of India: Current Science, v. 88, no. 8, p. 1297-1301

Clague, JJ, Bobrowsky, PT, and Hamilton, TS, 1994. A sand sheet deposited by the 1964 Alaska tsunami at Port Alberni, British Columbia. Estuarine, Coastal and Shelf Science 38, 413–421.

Dawson, AG, Long, D, and Smith, DE, 1988, The Storegga Slides - Evidence from Eastern Scotland for a Possible Tsunami: Marine Geology, v. 82, p. 271-276.

Dawson, AG and Shi, S, 2000, Tsunami Deposits: Pure and Applied Geophysics, v. 157, p. 875-897.

Fedotov, SA, Ivanov, B, Avdeyko, GP, Flerov, GB, Andreyev, VN, Dvigalo, VN, Dubik, YM, and Chirkov, AM, 1981, Izverzheniye vulkana Alaid v 1981 g.. The Alaid Volcano eruption in 1981, Vulkanologiya i Seysmologiya, vol.1981, no.5, pp.82-87.

Fedotov, SA, Chernyshev, SD, and Chernysheva, GV, 1982, The Improved Determination of the Source Boundaries for Earthquakes of M >7.75, of the Properties of the Seismic Cycle, and of Long-term Seismic Prediction for the Kurile-Kamchatka Arc: Earthquake Prediction Research, v. 1, p. 153-171.

Geist, EL, 2002, Complex earthquake rupture and local tsunamis, Journal of Geophysical Research, v. 107, doi:10.1029/2000JB000139

Geist, EL and Dmowska, R, 1999, Local tsunamis and distributed slip at the source, Pure and Applied Geophysics, v. 154, p. 485-512.

Hindson, RA, and Andrade, C, 1999, Sedimentation and hydrodynamic processes associated with the tsunami generated by the 1755 Lisbon earthquake: Quaternary International, v. 56 , p. 27-38.

Hirata, K, Geist, E, Stake, K, Tanioka, Y, and Yamaki, S, 2003, Slip distribution of the 1952 Tokachi-Oki earthquake (*M* 8.1) along the Kuril Trench from tsunami waveform inversion, Journal of Geophysical Research, v. 108, doi:10.1029/2002JB001976.

Hodgson, JH, 1956, Direction of Faulting in Some of the Larger Earthquakes of the North Pacific, 1950-1953: Publ. Dom. Obs. Ottawa, v. 18, p. 219-252.

Hutchinson, RO, 1954, The Kamchatka Earthquakes of November, 1952: Earthquake Notes, v. 25, p. 37-41.

Ishii M, Shearer PM, Houston H, and Vidale, JE, 2005, Extent, duration and speed of the 2004 Sumatra-Andaman earthquake imaged by the Hi-Net array, Nature, v. 435, n. 7044, p. 933-936.

Johnson, JM, Holdahl, SR, and Satake, K, 1997, The 1964 Prince William Sound earthquake: joint inversion of tsunami and geodetic data, Journal of Geophysical Research, v. 101, p.523-532.

Johnson, JM, and Satake, K, 1996, Asperity distribution of Alaska-Aleutian earthquakes: implications for seismic and tsunami hazards, *in* G. Hebenstreit (*ed*.), Perspectives on tsunami hazard reduction, Netherlands, Kluwer Academic Publishers, p. 67-81

Johnson, JM, and Satake, K, 1999, Asperity distribution of the 1952 great Kamchatka earthquake and its relation to future earthquake potential in Kamchatka, Pure and Applied Geophysics, v. 154, no. 3-4, p.541-553.

Kanamori, H, 1976, Re-examination of the Earth's free oscillations excited by the Kamchatka earthquake of November 4, 1952, Physics of the Earth and Planetary Interiors, v. 11, no. 3, p. 216-226.

Kanamori, H, 1972, Mechanism of tsunami earthquakes Physics of the Earth and Planetary Interiors, v.6, no.5, p.346-359.

Kelleher, J, and Savino, J, 1975, Distribution of Seismicity before Large Strike Slip and Thrust-type Earthquakes: Journal of Geophysical Research, v. 80, p. 260-271.

Kelsey, HM, Witter, RC, and Hemphill-Haley, E, 2002, Plate-boundary earthquakes and tsunamis of the past 5500 yr, Sixes River estuary, southern Oregon: Geological Society of America Bulletin, v. 114, p. 298-314.

Lay T, Kanamori H, Ammon CJ, Nettles M, Ward SN, Aster RC, Beck SL, Bilek SL, Brudzinski MR, Butler R, DeShon HR, Ekstrom G, Satake K, and Sipkin S, 2005, The great Sumatra-Andaman earthquake of 26 December 2004: Science, v. 308, p. 1127-1133.

Melekestsev IV, Braitseva OA, Dvigalo VN, and Bazanova LI, 1994, Historical eruptions of Avacha volcano, Kamchatka: Attempt of modern interpretation and classification for long-term prediction of the types and parameters of future eruptions. Part 2 (1926-1991). Volc Seism, 16: 93-114 (English translation)

Minoura, K, Gusiakov, VG, Kurbatov, A, Takeuti, S, Svendsen, JI, Bondevik, S, and Oda, T, 1996, Tsunami sedimentation associated with the 1923 Kamchatka earthquake. Sedimentary Geology 106, 145–154.

Nanayama, F, Furukawa, R, Shigeno, K, Makino, A, Soeda, Y, and Igarashi, Y., *in press,* Nine unusually large tsunami deposits from the past 4000 years at Kiritappu march along the southern Kuril trench: Sedimentary Geology.

Nanayama F, Satake K, Furukawa R, Shimokawa K, Atwater BF, Shigeno K, and Yamaki S, 2003, Unusually large earthquakes inferred from tsunami deposits along the Kuril trench: Nature, v. 424, no. 6949, p. 660-663.

Nanayama, F, Shigeno, K, Satake, K, Shimokawa, K, Koitabashi, S, Miyasaka, S, and Ishii, M, 2000, Sedimentary differences between the 1993 Hokkaido-nansei-oki tsunami and the 1959 Miyakojima typhoon at Taisei, southwestern Hokkaido, northern Japan, Sedimentary Geology, 135, 255-264.

Nikonov, AA, 2006, Kuril'skaya katastrofa 1952 g., vyzvannaya tsunami. (Kuril catastrophe in 1952 caused by tsunami), Izvestiya Akademii Nauk, Rossiyskaya Akademiya Nauk, Seriya Geograficheskaya, v. 2006, n. 2, p. 48-58. [in Russian]

Okada, R, 1985, Surface deformation due to shear and tensile faults in a half-space, Bulletin of the Seismological Society of America, v. 75, n. 4, p. 1135-1154.

Okal, E., 1992, Use of Mantle Magnitude Mm for the Reassessment of the Moment of Historical Earthquakes I: Shallow Events: Pure and Applied Geophysics, v. 139, p. 17-57.

Ovsyannikov AA, and Muraviev YD, 1992. The 1986 eruption of Chikurachki volcano. Volc Seism, v. 5-6, pp. 3-20 (English tranlation 1993, 14: 493-514)

Pinegina, TK, Bourgeois, J, Bazanova, LI, Melekestsev, IV, and Braitseva, OA, 2003, A millennial-scale record of Holocene tsunamis on the Kronotskiy Bay coast, Kamchatka, Russia, Quaternary Research, 59, 36–47.

Pinegina, TK, and Bourgeois, J, 2001, Historical and paleo-tsunami deposits on Kamchatka, Russia; long-term chronologies and long-distance correlations: Natural Hazards, v. 1, p. 177-185.

Satake, K, Nanayama, F, Yamaki, S, Tanioka, Y, and Hirata, K, 2005, Variability among tsunami sources in the 17th-21st centuries along the southern Kuril Trench; Tsunamis; case studies and recent developments: Advances in Natural and Technological Hazards Research, v. 23, p. 157-170.

Titov, VV and Gonzales, FI, 1997, Implementation and testing of the methods of splitting tsunami (MOST) model. Technical Report NOAA Tech. Memo. ERL PLEL-112 (PB98-122773), NOAA/Pacific Marine Environmental Laboratory, Seattle, WA.

Titov, VV, Gonzales, FI, Bernard, EN, Eble, MC, Mofjeld, HO, Newman, JC, and Venturato, AJ , 2005, Real-time tsunami forecasting: challenges and solutions: Natural Hazards, v. 35, p. 41-58.

Titov, VV, Mofjeld, HO, Gonzales, FI, and Newman, JC , 2001, Offshore forecasting of Alaskan tsunamis in Hawaii. In: G.T. Hebenstreit (ed.), Tsunami Research at the End of a Critical Decade. Birmingham, England, Kluwer Acad. Pub., Netherlands, pp. 75-90.

Titov, VV and Synolakis, CE, 1998, Numerical modeling of tidal wave runup, Journal of Waterway, Port, Coastal and Ocean Engineering, v. 124, p. 157-171.

Titov, VV and Synolakis, CE, 1996, Numerical modeling of 3-D long wave runup using VTCS-3. In: Yeh, H., Liu, P., and Synolakis, C. (*eds*), Long wave runup models. Singapore, World Scientific Publishing Co. Pte. Ltd., p. 242-248.

Titov, VV and Synolakis, C.E., 1995, Modeling of breaking and nonbreaking long-wave evolution and runup using VTCS-2. Journal of Waterways, Ports and Ocean Engineering, v. 121, p. 308-316.

Weiss, R, Sediment grains moved by passing tsunami waves: Tsunami deposits in deep water, Marine Geology, *in press*

Zayakin, YA, and Luchinina, AA, 1987, Catalogue of tsunamis on Kamchatka: Obninsk, Vniigmi-Mtsd, 50 p. (in Russian)

Table 1: Tsunamigenic earthquakes in the northern Kuril-Kamchatka subduction zone (see Fig. 1). Data obtained from the Historical Tsunami Database for the Pacific (HTDB/PAC) which is not yet updated to include the 2006 Kuril Island earthquake.

Earthquake					**Tsunami**	
Year	Month	Day	M_w	M_t	Elevation in field area (m)	Total world observations
1737	10	17	x	x	27-63	7
1792	8	22	x	x	x	2
1841	5	17	x	9	1-15	7
1904	6	25	7.6	x	x	1
1917	1	30	7.6	x	x	1
1923	2	3	8.6	8.8	x	39
1952	11	4	9	9	2-18	339
1959	5	4	8	8	0.01-2	12
1960	5	22	9.5	9.4	1-7	630
1971	12	15	7.8	7.8	0.1-0.36	15
1993	6	8	7.5	7.5	x	5
1997	12	5	7.7	7.8	x	14

Figure Captions:

Figure 1: Location and seismicity of Kamchatka and the northern Kuril Islands. Numbers and circles refer to the year and presumed rupture area of tsunamigenic subduction-zone earthquakes. Rupture zones or epicenters for two events in the 18^{th} century are unknown. Refer to Table 1 for more information.

Figure 2: Major aftershocks of the 1952 event and the preferred slip distribution determined by Johnson and Satake, 1999. Aftershocks help define the rupture area.

Figure 3: The calculation of the tsunami deposit estimate (TDE) of minimum wave height. A: An example of a profile with the sediment limit of inundation. The profile is zeroed at high-high tide. The TDE is determined from the elevation of the highest deposit. No slope is given to the tsunami as that requires additional assumptions about tsunami wave behavior. B: An example profile where the tsunami inundates farther than the profile. The topography beyond the end of the profile is unknown. C: TDE values for every profile or cataloged observation. The black line indicates the highest observation for every embayment or general area and represent the minimum height to which a tsunami must have reached in order to explain all of the deposits and cataloged data.

Figure 4: Location of unit sources (outlined in black) and model grids in relation to Kamchatka and the 1952 rupture area. The tsunami initially propagates through the 120" resolution grid. The larger grid provides the input at the edges of the 30" resolution grids in which tsunami runup is calculated.

Figure 5: A comparison of TDE and TMA values from source models with equal slip distributed through the entire rupture area or in shallow or deep concentrations. For discussion, see section 4.2.

Figure 6: A comparison of TDE and TMA values from source models with equal slip distributed in localized regions, north-south through the subduction zone. For discussion, see section 4.2.

Figure 7: A comparison of TDE and TMA values from source models proposed by Johnson and Satake, 1999. The minimum and maximum slip distributions are a result of the reported error range in slip. The M_w 9.0 model increases the slip of the M_w 8.8 model but keeps the ratio of slip distribution the same. For discussion, see section 4.3.

Figure 8: A comparison of TDE and TMA values from source models that have minor alterations between them. These models are based on the Johnson and Satake, preferred slip distribution. For discussion, see section 4.3.

Figure 1:

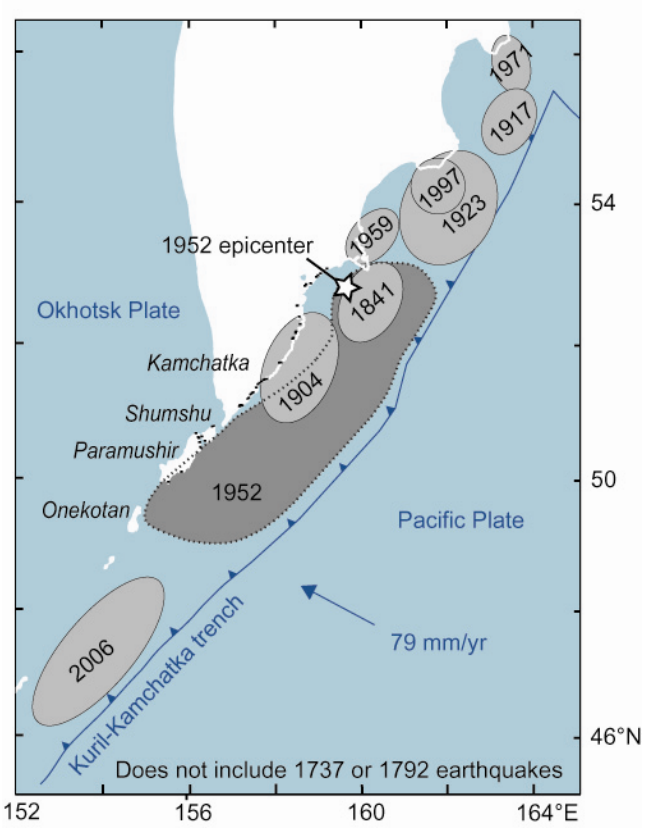
1971
1917
1997
1923
1959
1952 epicenter
1841
Okhotsk Plate
Kamchatka
1904
Shumshu
Paramushir
1952
Onekotan
Pacific Plate
79 mm/yr
2006
Kuril-Kamchatka trench
Does not include 1737 or 1792 earthquakes
54
50
46°N
152
156
160
164°E

Figure 2:

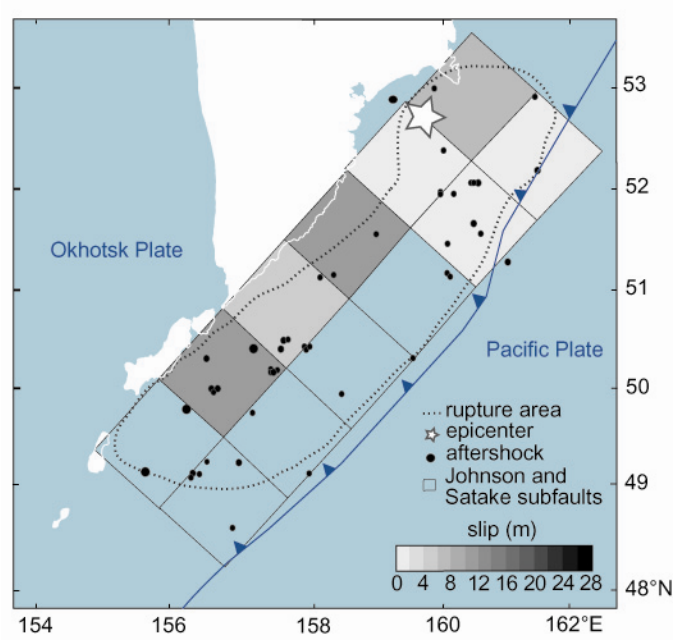
Okhotsk Plate
Pacific Plate
rupture area
epicenter
aftershock
Johnson and Satake subfaults
slip (m)
0 4 8 12 16 20 24 28
53
52
51
50
49
48°N
154
156
158
160
162°E

Figure 3:

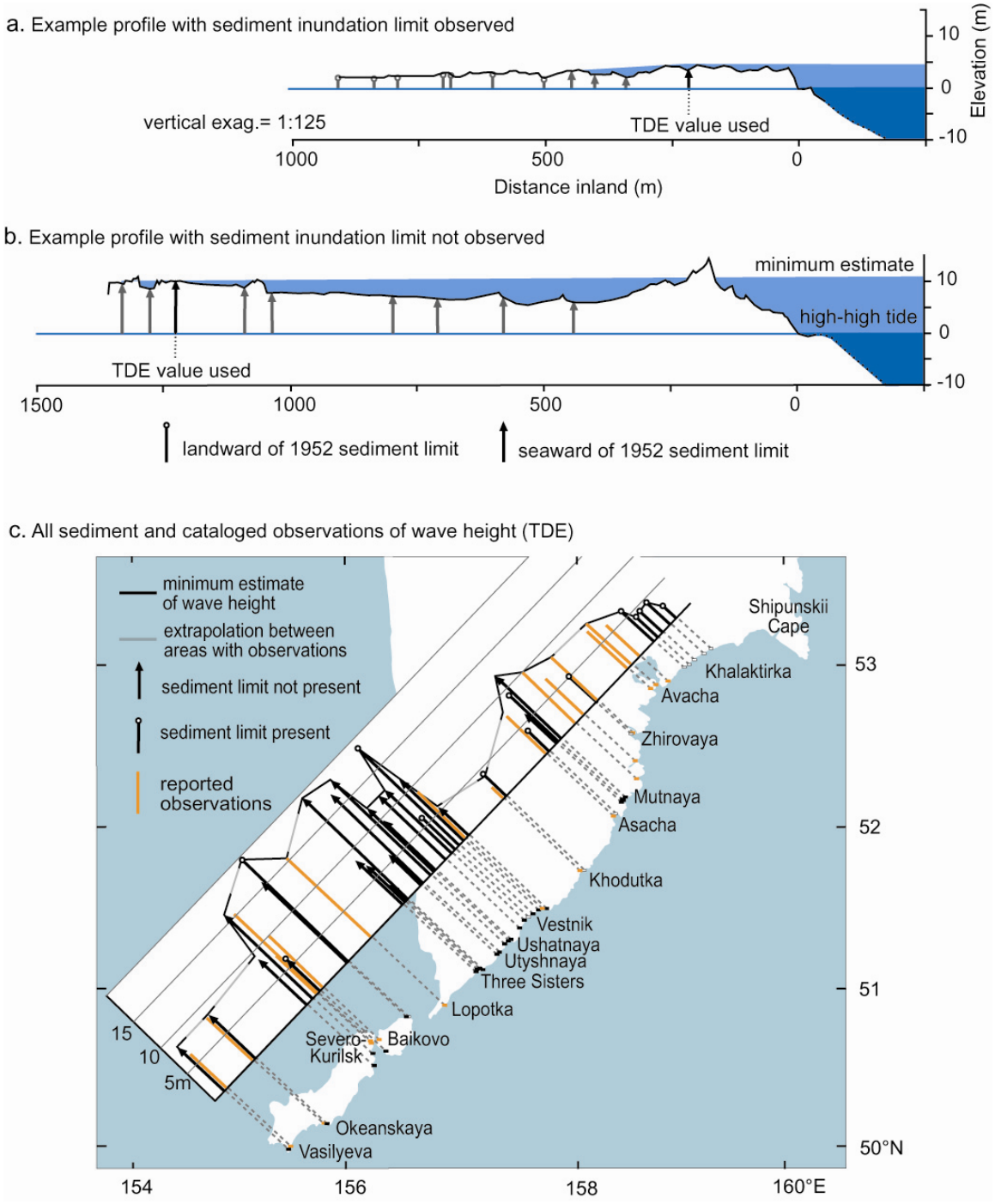
a. Example profile with sediment inundation limit observed
vertical exag.= 1:125
TDE value used
1000
500
0
Distance inland (m)
10
0
-10
Elevation (m)
b. Example profile with sediment inundation limit not observed
minimum estimate
high-high tide
TDE value used
1500
1000
500
0
landward of 1952 sediment limit
seaward of 1952 sediment limit
c. All sediment and cataloged observations of wave height (TDE)
minimum estimate of wave height
extrapolation between areas with observations
sediment limit not present
sediment limit present
reported observations
15
10
5m
Shipunskii Cape
Khalaktirka
Avacha
Zhirovaya
Mutnaya
Asacha
Khodutka
Vestnik
Ushatnaya
Utyshnaya
Three Sisters
Lopotka
Severo-Kurilsk
Baikovo
Okeanskaya
Vasilyeva
53
52
51
50°N
154
156
158
160°E

Figure 4:

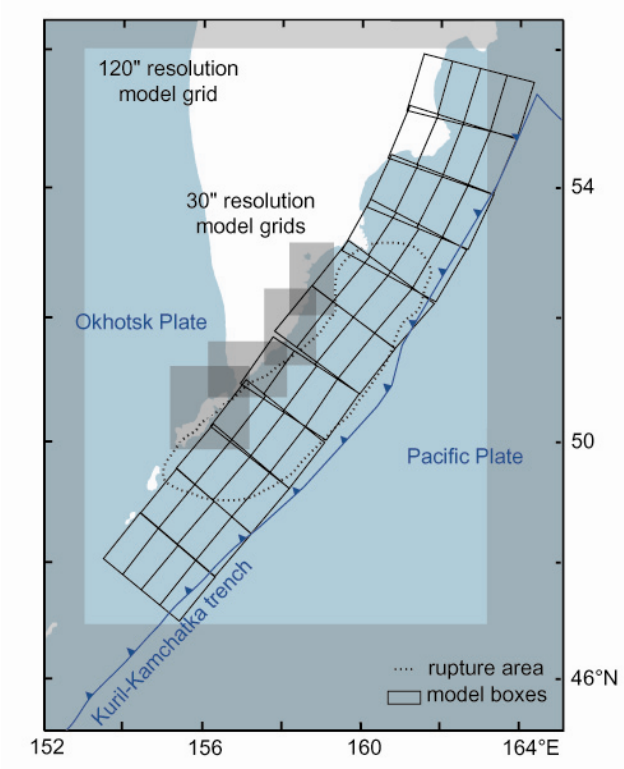
120" resolution
model grid
30" resolution
model grids
Okhotsk Plate
Pacific Plate
Kuril-Kamchatka trench
rupture area
model boxes
54
50
46°N
152
156
160
164°E

Figure 5:

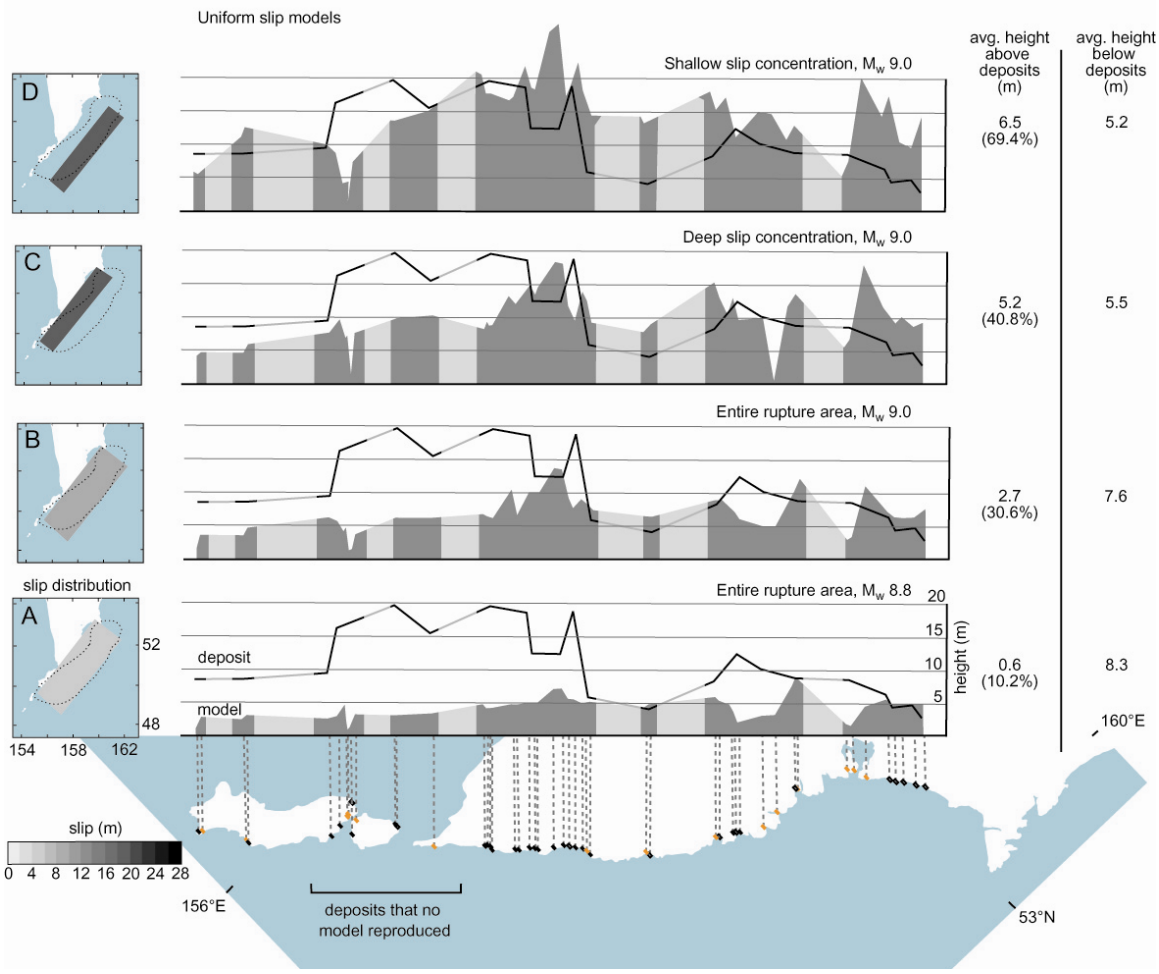
Uniform slip models
Shallow slip concentration, M_w 9.0
Deep slip concentration, M_w 9.0
Entire rupture area, M_w 9.0
Entire rupture area, M_w 8.8
avg. height above deposits (m)
avg. height below deposits (m)
6.5 (69.4%)
5.2
5.2 (40.8%)
5.5
2.7 (30.6%)
7.6
0.6 (10.2%)
8.3
D
C
B
A
slip distribution
52
48
154
158
162
deposit
model
20
15
10
5
height (m)
160°E
slip (m)
0 4 8 12 16 20 24 28
156°E
deposits that no model reproduced
53°N

Figure 6:

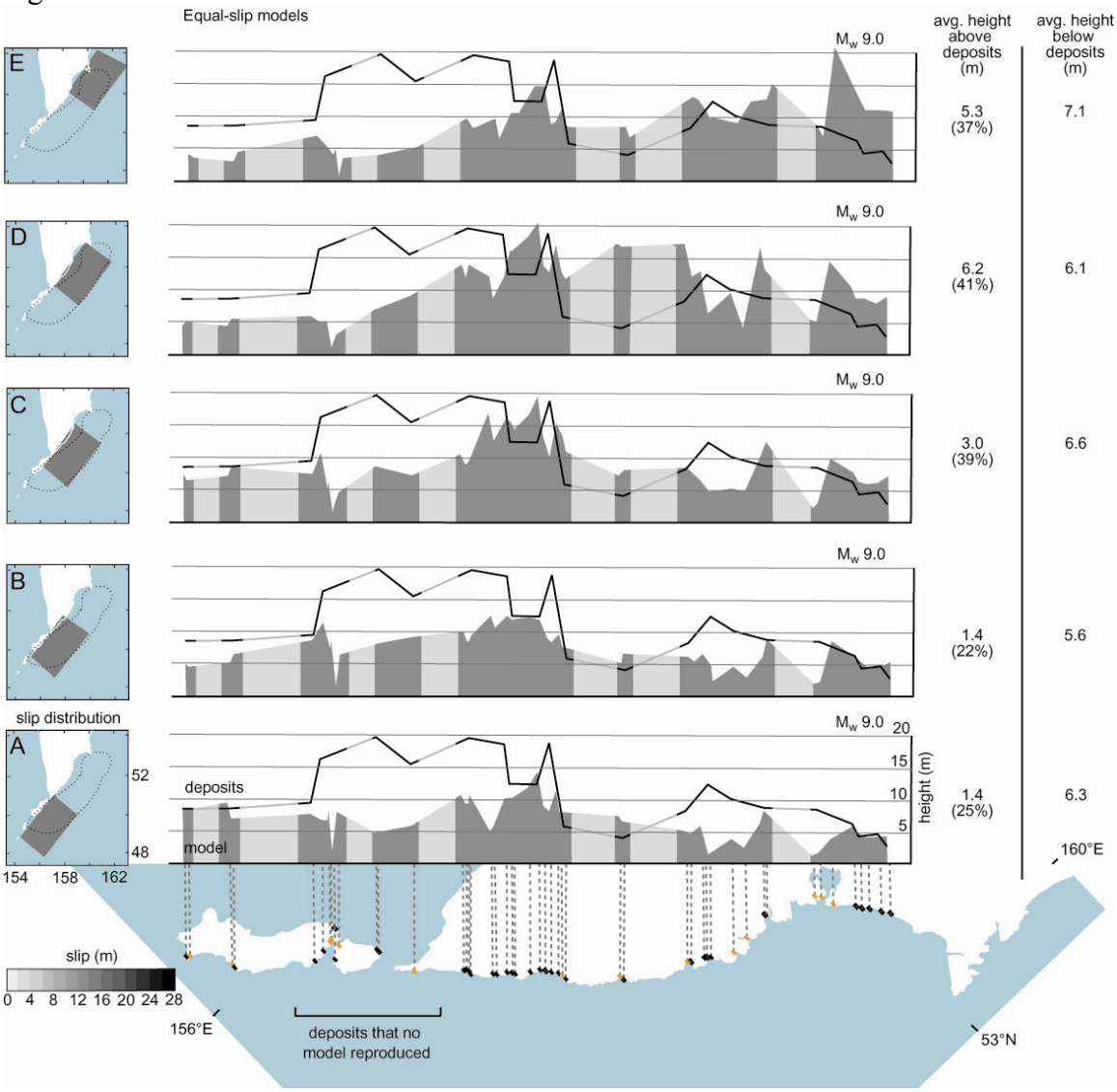
Equal-slip models
avg. height above deposits (m)
avg. height below deposits (m)
E
D
C
B
A
M_w 9.0
5.3 (37%)
7.1
6.2 (41%)
6.1
3.0 (39%)
6.6
1.4 (22%)
5.6
1.4 (25%)
6.3
slip distribution
52
48
154
158
162
deposits
model
20
15
10
5
height (m)
160°E
slip (m)
0 4 8 12 16 20 24 28
156°E
deposits that no model reproduced
53°N

Figure 7:

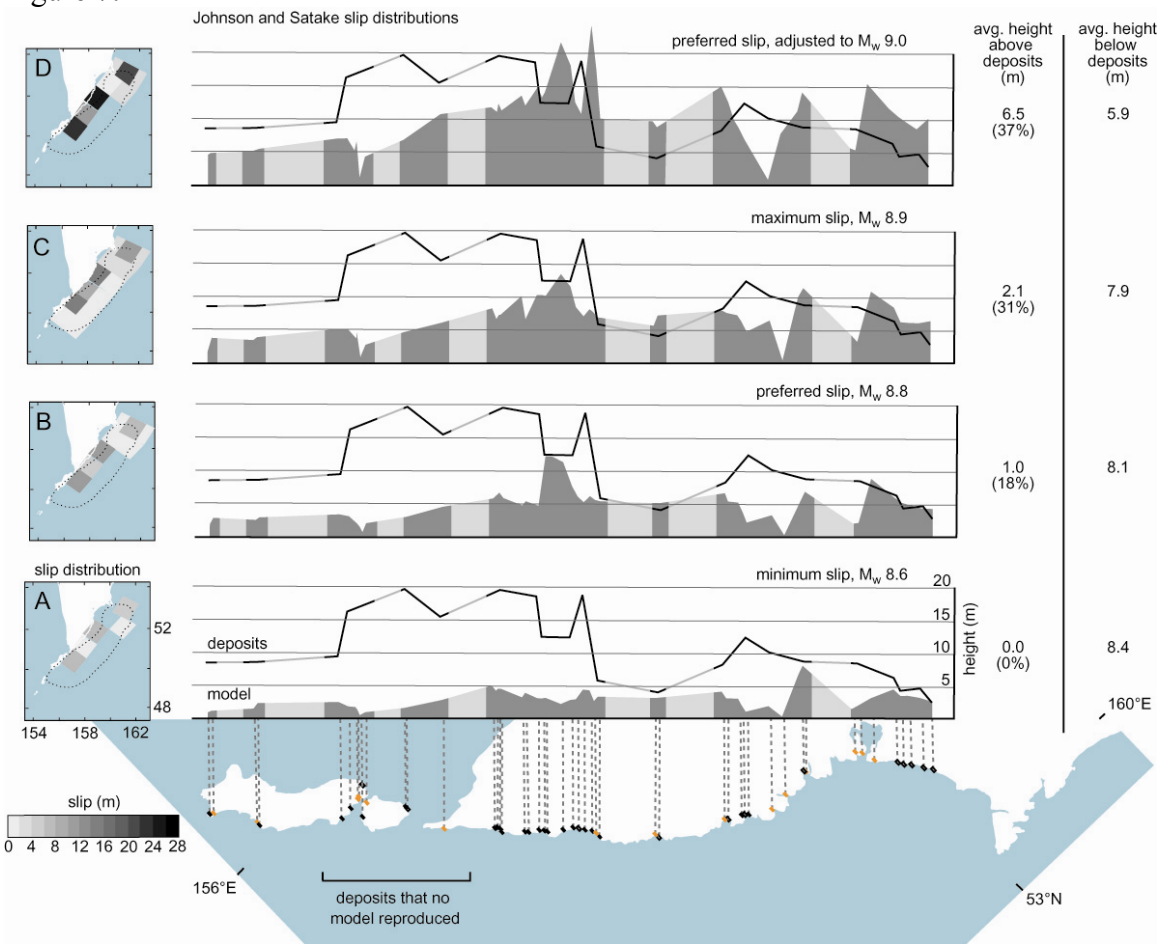
Johnson and Satake slip distributions
preferred slip, adjusted to M_w 9.0
avg. height above deposits (m)
avg. height below deposits (m)
6.5 (37%)
5.9
D
maximum slip, M_w 8.9
2.1 (31%)
7.9
C
preferred slip, M_w 8.8
1.0 (18%)
8.1
B
slip distribution
minimum slip, M_w 8.6
20
15
10
5
height (m)
A
52
48
deposits
model
0.0 (0%)
8.4
154
158
162
160°E
slip (m)
0 4 8 12 16 20 24 28
156°E
deposits that no model reproduced
53°N

Figure 8:

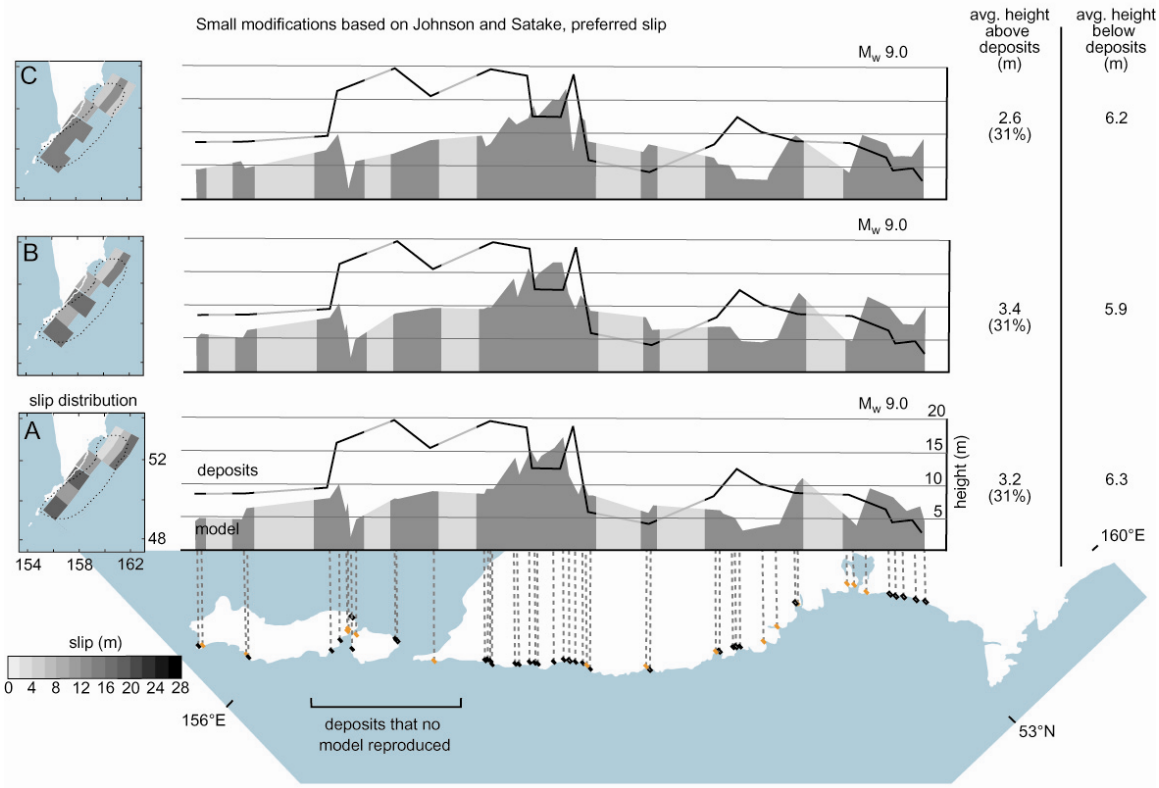
Small modifications based on Johnson and Satake, preferred slip
avg. height above deposits (m)
avg. height below deposits (m)
C
B
A
slip distribution
M_w 9.0
M_w 9.0
M_w 9.0
2.6 (31%)
6.2
3.4 (31%)
5.9
3.2 (31%)
6.3
deposits
model
height (m)
20
15
10
5
52
48
154
158
162
160°E
slip (m)
0 4 8 12 16 20 24 28
156°E
deposits that no model reproduced
53°N